6 January 2026

# Interfacial Self-Assembly of Graphene Networks at 1 vol % Enables Piezoresistive and Electrothermal Silicone Foams

Brenden Ferland[1], Douglas Adamson[1]

1. University of Connecticut

## Abstract

Segregated network composites achieve electrical percolation at minimal filler loadings by localizing conductivity to architectural boundaries. However, achieving this architecture typically requires tedious multi-step processing, often incompatible with scalable manufacturing. Here, we report the single-step synthesis of a silicone composite segregated network composed of self-assembled percolating graphene networks. These networks are templated by graphene-stabilized water-in-oil emulsions, created by spontaneous exfoliation of graphite at oil/water interfaces generated by agitation. After polymerization of the silicone and removal of the dispersed aqueous phase, the resulting foams achieve conductivities of 0.43 S/m at a 1.37 vol% loading of graphene. This is a 12-fold reduction compared to prior interfacial assembly methods, which require 16.5 vol% loading and thousands of hours of processing to achieve comparable electrical conductivity. Architectural segregation decouples mechanical and electrical properties, enabling application-specific modulus tuning. The foams exhibit reversible piezoresistance with a U-shaped strain response, are stable through 5000 cycles, and provide voltage-controlled heating to 143 °C at milliamp current densities, three orders of magnitude lower than those of continuous CVD graphene networks. The low thermal mass of the air-filled foam structure provides rapid thermal response, achieving 28-second de-icing from -17 °C.

## Keywords

graphene, silicone foam, polyHIPE, piezoresistive, percolation, emulsion templating, conductive composite, strain sensing, self-assembly, electrothermal

# Interfacial Self-Assembly of Graphene Networks at 1 vol% Enables Piezoresistive and Electrothermal Silicone Foams

**Brenden Ferland**[1] **and Douglas Adamson**[1,2,*]

[1]Polymer Program, Institute of Materials Science, University of Connecticut, Storrs, CT 06269; [2]Department of Chemistry, University of Connecticut, Storrs, CT 06269

**Abstract** Segregated network composites achieve electrical percolation at minimal filler loadings by localizing conductivity to architectural boundaries. However, achieving this architecture typically requires tedious multi-step processing, often incompatible with scalable manufacturing. Here, we report the single-step synthesis of a silicone composite segregated network composed of self-assembled percolating graphene networks. These networks are templated by graphene-stabilized water-in-oil emulsions, created by spontaneous exfoliation of graphite at oil/water interfaces generated by agitation. After polymerization of the silicone and removal of the dispersed aqueous phase, the resulting foams achieve conductivities of 0.43 S/m at a 1.37 vol% loading of graphene. This is a 12-fold reduction compared to prior interfacial assembly methods, which require 16.5 vol% loading and thousands of hours of processing to achieve comparable electrical conductivity. Architectural segregation decouples mechanical and electrical properties, enabling application-specific modulus tuning. The foams exhibit reversible piezoresistance with a U-shaped strain response, are stable through 5000 cycles, and provide voltage-controlled heating to 143 °C at milliamp current densities, three orders of magnitude lower than those of continuous CVD graphene networks. The low thermal mass of the air-filled foam structure provides rapid thermal response, achieving 28-second de-icing from −17 °C.

*E-mail: Adamson@uconn.edu

**Keywords:** graphene, silicone foam, polyHIPE, piezoresistive, percolation, emulsion templating, conductive composite, strain sensing, self-assembly, electrothermal

## Introduction

Conductive elastomers (CE) face a fundamental constraint: adding conductive fillers compromises the mechanical compliance that makes them valuable. Emerging applications require materials that maintain electrical performance under substantial mechanical strain.[1–3] These applications range from prosthetic limbs with integrated tactile feedback[4, 5] to epidermal sensors that conform to dynamic tissue deformation.[6] Silicone elastomers are especially attractive for flexible electronics due to their exceptional chain flexibility, characterized by glass transition temperatures typically below −120 °C, coupled with thermal stability exceeding 300 °C,[7] chemical resistance, and biocompatibility.

However, silicones, like all elastomers, are electrical insulators (conductivity ≈ $10^{-12}$ S/m).[8] Traditional approaches to making them electrically conductive often use metallic fillers that, while highly conductive ($10^5$–$10^6$ S/m),[9] require high loadings for percolation, resulting in brittle materials ill-suited for flexible applications with drastically increased modulus, reduced elongation, and elevated viscosity, which complicates processing and undermines flexibility.

The percolation thresholds required to make useful CE materials with carbon nanotube and graphite nanoplatelet fillers are much lower, typically ranging from 0.1 to 10 vol%, depending on filler dispersion, aspect ratio, and processing conditions.[10, 11] However, these fillers are often costly or require hazardous, complex approaches to synthesize and disperse, creating challenges for scalability in manufacturing.[12, 13] These challenges are compounded with silicone because of the general non-wettability of silicone materials and the uniquely flexible Si–O bond that promotes filler aggregation rather than dispersion due to strong van der Waals forces between conductive filler particles.[14, 15]

Porous foam architectures offer a potential route to address these challenges through architectural control of filler distribution. By localizing conductive fillers at foam interfaces, segregated networks can achieve electrical percolation at lower overall filler loadings than uniform dispersion approaches, thereby preserving bulk mechanical compliance while establishing conductive pathways.[16] Numerous strategies have been explored to fabricate conductive graphene-silicone composite foams, each encountering specific limitations. For instance, the use of sacrificial templating requires multi-step processing, and filler dispersion is challenging.[17]

Chemical foaming methods offer simpler one-step processes, but they lack control over pore morphology and filler distribution, typically resulting in only moderate conductivities.[18] Freeze-drying processes yield ultralight and conductive aerogel structures, but require complex solvent-exchange protocols, and mechanically fragile materials are often produced.[19] Direct ink writing (DIW) affords precise spatial control of material architecture; however, it remains constrained to specific geometries and is challenging to scale.[20] These conventional techniques struggle to adequately address the fundamental challenge of controlling graphene dispersion and assembly at the micron-level, resulting in compromised mechanical-electrical performance.

Surprisingly few recent efforts have been reported to develop new interfacial assembly strategies that address these fabrication and performance challenges in silicone elastomers. O'Mara et al. [21] previously demonstrated graphene-silicone composites using an interfacial assembly approach to produce graphene by sonication, with piezoresistive capabilities, achieving conductivities approaching 1 S/m and tensile gauge factors of ~20, with strain sensing up to 80%. However, practical implementation was limited by interdiffusion periods exceeding 2,500 hours, the requirement of substantial solvent dilution, and graphene loadings reaching 16.5 vol% for optimal performance. Complementary work by Ogilvie et al. [22] demonstrated graphene-silicone composites with ultralow loading and relatively high conductivities of up to ~0.1 S/m via oil-in-water emulsion templating, establishing fundamental principles for surface-energy-controlled nanosheet stabilization. However, their approach yielded discrete silicone droplets embedded within a composite matrix, creating conductivity saturation at ~0.1 S/m due to interdroplet junction resistance inherent to the discontinuous architecture. This performance ceiling highlighted a trade-off between minimizing loading and improving electrical transport efficiency in segregated composite systems.

Continuous network architectures that employ chemical vapor deposition (CVD)-grown graphene foams infiltrated with polymer, providing uninterrupted transport pathways, have also been reported.[23] The performance-scalability trade-offs are manifest most clearly in current density requirements. Continuous CVD-grown graphene networks achieved conductivities approaching 500 S/m, operating in high-current, low-voltage regimes (above 1 A/cm$^3$),[23] but vacuum-based synthesis above 1000 °C creates prohibitive scaling barriers, and continuous phonon pathways reduce thermal efficiency. Dispersed architectures circumvent the complexity of CVD processing by incorporating pre-synthesized graphene, yet require a strategic compromise between conductivity and filler loading. Mechanical dispersion achieved ~110 S/m at 3.6 vol%, sufficient for thermal applications,[24] but limited by feedstock synthesis constraints, while laser-induced approaches demonstrated efficient heating (>11 °C/s) at modest voltages, though remained process-limited.

To meet these challenges, we hypothesized that segregated architectures formed through in-situ graphene exfoliation and self-assembly could circumvent both the manufacturing limitations of CVD networks and the feedstock requirements of dispersed systems. We previously demonstrated that graphite exfoliates to graphene at oil/water interfaces and stabilizes water-in-oil emulsions. These emulsions consist of water droplets stabilized against coalescence by a film of overlapping graphene sheets along with some unexfoliated graphite flakes pinned to the interface. This solvent interface trapping method (SITM) is thermodynamically driven, as graphene sheets act as two-dimensional surfactants, lowering the system's free energy.[25] The approach results in electrically conductive graphene-stabilized high internal phase emulsions (HIPEs).[25–27] Step-growth polymerization of the oil phase created an electrically conducting foam composite after removal of the dispersed water phase, with graphene films forming segregated conductive pathways.

This approach enabled the integration of both piezoresistive sensing and electrothermal heating within a single material, as both sensing and heating depend critically on percolation pathway connectivity and interfacial architecture, with thermodynamically driven assembly providing micron-level control over filler distribution. The present study demonstrates SITM-derived graphene-silicone polyHIPE foams that address the performance-scalability tension through in-situ graphene assembly during emulsion formation, followed by the hydrosilylation of the PDMS. This benchtop approach achieved electrical percolation at 1.0 vol%, reaching 0.43 S/m at 1.37 vol% compared to 16.5 vol% required in previous interfacial

assembly systems.[21]

## Results and Discussion

The synthesis and hierarchical assembly mechanism of piezoresistive silicone-graphene foams via SITM is illustrated in Scheme 1.

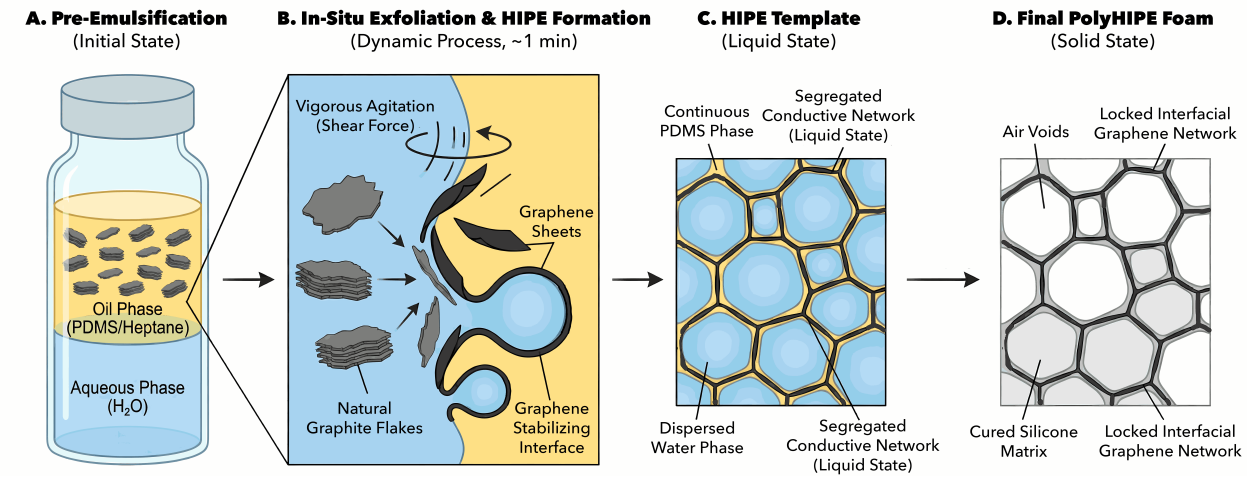


**Scheme 1. One-pot synthesis of conductive silicone-graphene foams via the Solvent Interface Trapping Method (SITM).** (A) Initial biphasic system comprising aqueous phase, polydimethylsiloxane (PDMS)/heptane oil phase, and natural graphite flakes. (B) Vigorous agitation (~1 min) disperses water droplets in oil and drives graphite migration to the oil/water interface, where thermodynamic forces induce exfoliation; the resulting graphene sheets act as 2D surfactants stabilizing water droplets. (C) High Internal Phase Emulsion (HIPE) template with graphene localized predominantly at interfaces, forming a percolating network. (D) Final polyHIPE foam after platinum-catalyzed curing and water removal, yielding a cellular silicone matrix with a segregated conductive graphene network lining cell walls.

### Morphological Characterization

The hierarchical structure of the graphene-silicone polymerized high internal phase emulsion (polyHIPE) foams was examined using scanning electron microscopy (SEM) (Figure 1). The foam exhibited a predominantly closed-cell architecture. At low magnification (Figure 1A), the cellular structure displayed cell diameters ranging from 50 to 500 µm, consistent with the polydisperse nature of hand-shaken emulsions; complete size distribution statistics are provided in the Supplementary Information (Figure S2).

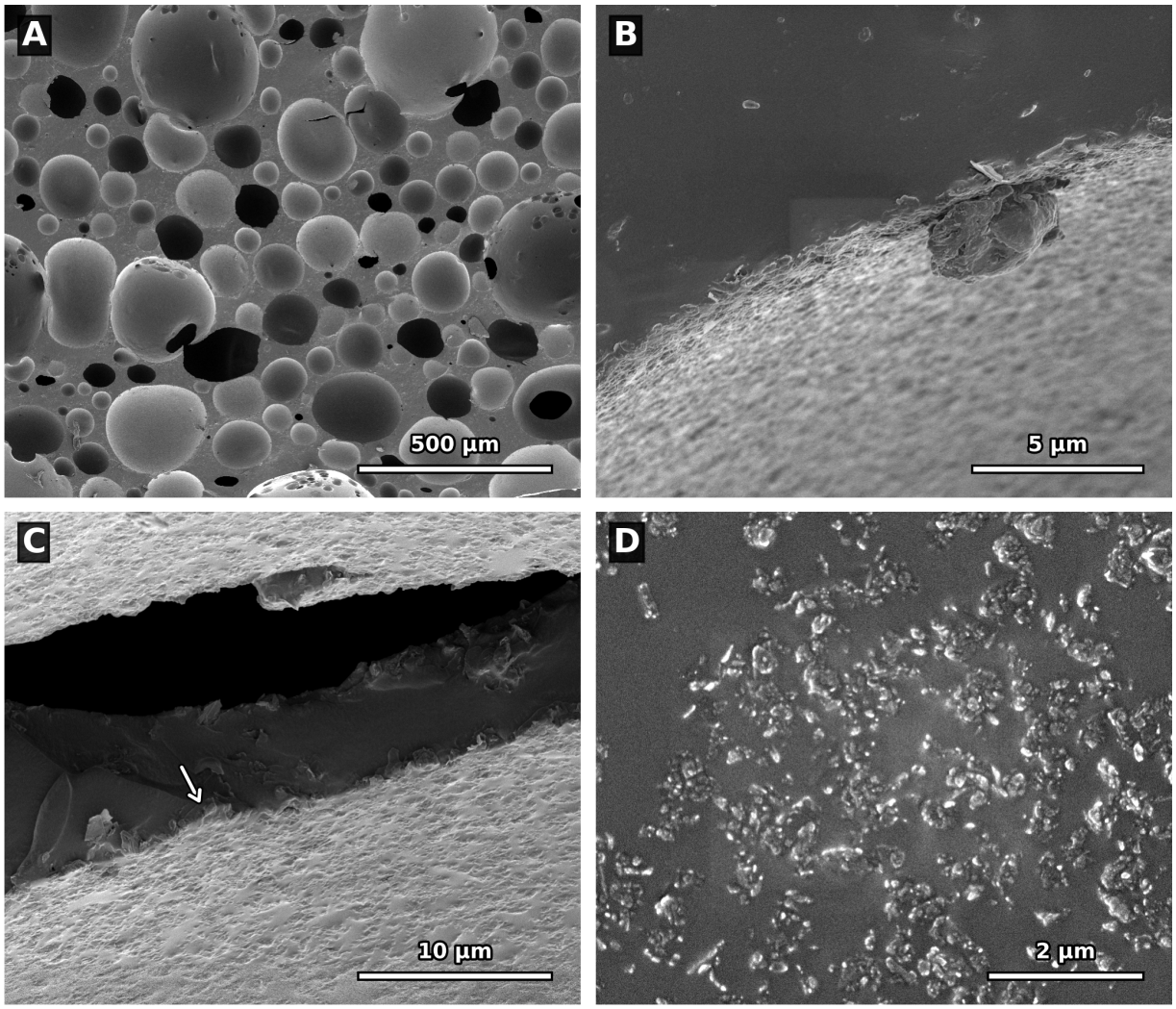


**Figure 1. Hierarchical morphology of graphene-stabilized silicone polyHIPE foams revealed by SEM.** (A) Low-magnification view showing polydisperse, predominantly closed-cell architecture produced by graphene-stabilized HIPE templating (scale bar: 500 µm). (B) Inter-cell junction showing graphene/graphite flakes jamming at the original water-oil interface, forming continuous bridges between adjacent pores that enable macroscopic electrical percolation (scale bar: 5 µm). (C) Cross-section of a cell wall exposing a ~1–2 µm graphene-rich lamina (dark, smooth band) flanked by rougher silicone regions; the fracture path and delamination void highlight this laminated structure as the mechanically weakest region and a potential low-tortuosity conduction plane (scale bar: 10 µm). (D) High-magnification image of pore bottom showing sub-micrometer graphene/graphite clusters within the cell wall matrix (scale bar: 2 µm). Alternate views of B & C are provided in Figure S3.

The interfacial exfoliation and assembly process generated a heterogeneous population of carbon structures, ranging from graphene to few-layer graphene (FLG) and residual graphite flakes. This structural diversity is characteristic of thermodynamically driven exfoliation, in which exfoliation stops once graphene sheets passivate the high-energy solvent/solvent interface. While this heterogeneity makes Raman spectroscopic analysis challenging, it provides functional advantages for electrical percolation by creating multiple conduction pathways with varying resistances. Higher magnification images of the cell lining (Figure 1B) revealed the overlapping graphene layers that formed at the oil/water interface and stabilized the emulsion template. Both individual graphene flakes and larger graphite particles are visible at the cell's surface, where they originally resided at the heptane/silicone-water interface during emulsification. These structures form continuous bridges between adjacent cells, creating a conductive pathway and electrical percolation throughout the foam structure.

Cross-sectional analysis of cell walls (Figure 1C) exposed a structure comprising a thin graphene-rich layer flanked by

silicone regions, which was exposed during sample preparation. The presence of delamination along this interface suggests that the graphene-silicone phase boundary represents a mechanically weak region within the cell walls, likely due to limited interpenetration between the silicone network and the graphene sheets. The ~1–2 μm graphene-rich lamina visible in cell wall cross-sections provides a low-tortuosity conduction plane, while the flanking silicone regions bear mechanical load. Also visible at the edges of the lower surface are graphene sheets that were exposed by tearing the sample during sample preparation, as annotated by a white arrow. These sheets are generally embedded in the polymer matrix and thus challenging to image directly. Higher-magnification imaging of the cell surface (Figure 1D) revealed submicrometer graphene/graphite clusters embedded within the cell wall, spanning the oil-water interface. These features resulted from graphene aggregates that remained at the interface during polymerization, contributing to the conductive network.

### Sphere Size Distribution Analysis

Quantitative cell-size analysis of graphene-stabilized silicone polyHIPE foams revealed greater cell-size uniformity than in polystyrene-based graphene-polyHIPEs.[26] The cumulative distribution function (Figure S2A) demonstrated that 90% of the spheres ($D_{90}$) fell below 176.4 μm, with a median diameter ($D_{50}$) of 84.3 μm and interquartile range spanning 60.1–132.3 μm ($D_{25}$–$D_{75}$). The volume fraction analysis (Figure S2B) revealed that while larger spheres (≥250 μm) dominated the volume fraction (approximately 62%), the number fraction was significantly different. The number fraction distribution (Figure S2C) showed that the greatest fraction was in the 50–100 μm range (approximately 43% by count), consistent with the measured median of 84.3 μm and indicating a substantial population of smaller spheres. Notably, the $D_{10}$ value of 45.1 μm indicated a significant presence of sub-50 μm spheres, contributing to the observed bimodal size distribution. This cellular size distribution was markedly different than previous SITM-derived polyHIPE systems. Our styrene-based foams exhibited average cell diameters of 230–255 μm,[26] while butyl acrylate foams ranged from 100–300 μm.[28] The decrease in cell size in the silicone matrix was attributed to the greater viscosity of the oil phase and faster polymerization in the silicone system, resulting in less aqueous droplet coalescence. Smaller cells increase the density of cell-cell junctions per unit volume; since electrical transport requires hopping between cells through overlapping graphene sheets, more junctions create more parallel conduction pathways, reducing bulk resistance. The smaller cells also distribute mechanical load across more cell walls, reducing local stress concentrations.

## Interfacial Behavior

We found that additive-free silicone formulations were necessary for successful SITM implementation, and we demonstrated this through comparative experiments with commercial silicone systems. When the additive-free Gelest macromer formulation was replaced with commercial Sylgard 184, the resulting HIPE-templated foams were macroscopically indistinguishable but electrically insulating ($\sigma < 10^{-6}$ S/m), even after reducing the resin viscosity with heptane dilution. Sylgard 184 contains a high loading of nanoscale fumed silica, approximately 30–60 wt%,[29] which disrupted the interfacial exfoliation through a competitive adsorption mechanism. The amphiphilic nature of those silica nanoparticles, with the capacity to reduce interfacial tension at oil-water boundaries,[30] created a direct competition with graphene exfoliation processes. Once adsorbed, these silica particles caused “interfacial crowding”[31–33] in which the high-density particle assemblies physically occupied sites required for graphite exfoliation, preventing the formation of electrically conductive graphene pathways.

This action of silica particles in our system was studied using hexamethyldisilazane (HMDZ) modification experiments, where HMDZ treatment renders silica particles more hydrophobic by replacing surface silanol groups with trimethylsilyl groups.[34] Mahadik et al. [35] showed that the interfacial tension increased to ~66 mN/m upon HMDZ treatment in silica aerogels. We found that the addition of the HMDZ-modified silica to our templating emulsions eliminated electrical conductivity in the final material. The increase in surface tension drove HMDZ-silica particles to minimize water contact by adsorbing to the oil-water interface. Literature reports suggest that through enhanced interfacial crowding, the modified particles prevent other species from adsorbing at the interface.[36] This is in contrast to unmodified, hydrophilic silica particles, where aqueous silica dispersions added to our emulsion templates resulted in electrically conductive final products. This is presumably due to the hydrophilic silica particles preferentially remaining in the aqueous phase rather than adsorbing at the oil-water interface.[37]

Direct observation (Figure S4) confirmed the accumulation of hydrophobic silica at the oil-water interface, providing visual evidence that surface chemistry governs competitive adsorption behavior and indirect evidence for the role of

graphite exfoliation at the oil/water interface in the electrical properties of the silicone composites. Percolation modeling of segregated composites indicates that even a few volume percent of nanoscale insulators can fragment a conductive network and increase bulk resistivity by orders of magnitude.[16, 38] Control experiments using additive-free PDMS confirmed that silicone matrix composition, rather than processing variables, determined electrical performance. Electrical conductivity required additive-free silicone; commercial formulations containing fumed silica produced insulating foams regardless of graphene loading.

In a related result, we found that successful synthesis and recovery of our composites required silanization of the reaction vessels due to the exceptionally strong adhesion between the graphene-containing composite and untreated glass surfaces. This adhesion often exceeded the foam's cohesive strength, leading to mechanical failure and fragmentation during demolding. This was unexpected, as pure PDMS typically exhibits poor glass adhesion and requires specialized adhesion promoters, such as allyltrimethoxysilane, to bond to silicate/glass surfaces.[39]

The enhanced adhesion observed in our graphene-silicone system is consistent with the adhesion energies reported for graphene-$SiO_2$ interfaces (0.31–0.45 $J{\cdot}m^{-2}$), which were attributed to van der Waals forces and 'liquid-like' conformability of graphene to $SiO_2$ topography.[40] This strong interfacial bonding likely arose from favorable interactions between graphene sheets and the glass interface, involving $\pi$-electron interactions with surface silanol groups and van der Waals forces between graphene basal planes and the silicate network. Surface passivation with dichlorodimethyl silane effectively eliminated this adhesion and preserved foam integrity for characterization. This strong glass-graphene-silicone interfacial bonding suggests potential applications where enhanced adhesion to glass substrates is desired, such as in electronic device encapsulation or structural composite applications where conventional silicone adhesion to glass is inadequate.

## Electrical Percolation

The electrical conductivity of the graphene-silicone foams prepared via SITM was systematically investigated as a function of graphite loading (Figure 2A). The conductivity measurements revealed a sharp percolation transition, as expected given the composite's segregated network. At low graphene loadings (0.36 and 0.66 vol%), the foams exhibited insulating behavior with electrical resistances exceeding the limitations of our Keithley 2400 instrument (~200 MΩ). Insulative samples had pervasive fissures, which impeded conductivity by creating large gaps. Percolation onset was determined to be between 0.66 and 1.04 vol%, but was likely more due to a cohesive structure than actual percolation onset. Above this percolation threshold, the samples are mechanically coherent. This achieves comparable conductivity (~0.4 S/m) at 1.37 vol% versus the 16.5 vol% required by prior interfacial assembly methods; a 12-fold reduction in filler loading.[21] For comparison purposes, a 4.66 vol% sample was synthesized. However, due to the extensive dilution required to compensate for viscosity and the high filler content paired with the porous architecture, the structural integrity of the sample was compromised. This resulted in a brittle, Swiss-cheese-like morphology, hampering further testing. Separately from graphene loading, we performed a series of adjustments to the crosslink density, ranging from 0.293 to 0.314 mmol vinyl $g^{-1}$ silicone, which modulated compressive modulus from 0.17 to 0.52 MPa (Figure S5). Electrical conductivity remained relatively constant across this range, indicating that the conductive network at cell interfaces is insensitive to bulk crosslink density.

Overall, the samples represented a conductivity span of nearly six orders of magnitude across the investigated loading range with a sharp transition from insulating to electrical percolation behavior. The percolation threshold of approximately 1.0 vol% and the subsequent rapid increase in conductivity at higher loadings are consistent with the formation of a continuous conductive network at cell interfaces. This percolation behavior is consistent with typical values reported for graphene-polymer composites, which commonly range from 0.05 to 2.5 vol% depending on the processing method, graphene type, and polymer matrix.[10]

The electrical properties of the silicone-graphene polyHIPE foams were attributable to the SITM-derived segregated network architecture. The filler was localized to cell walls via thermodynamically driven interface trapping, thereby dramatically increasing the local filler concentration at the cell wall. In addition to the localization of the filler, exfoliation of graphite to graphene at the oil/water interface introduced a tunneling electrical conduction mechanism.[41] The combination of both the segregated network, enhanced graphene conductivity, and ability to tunnel through insulating junctions resulted in a composite with superior conductivity at a much lower volumetric loading than previously reported similar technologies.

## Piezoresistive Response

The piezoresistive response of the silicone-graphene composite foams was evaluated using a cyclic compression test on an Instron 5869. Resistance was simultaneously monitored using a Keithley 2400 source measure unit (SMU) and a custom Python script. Figure 2C displays the electrical resistance over 5,000 cycles at 10% strain, with a cycle time of 6 seconds. The inset displays individual cycles at roughly the mid-point of the experiment. A distinct U-shaped response was observed (two peaks per compression cycle). In the beginning, resistance decreases and at an inflection point at ~6.68% strain, the resistance begins to increase, resulting in a positive piezoresistive regime that peaked at maximum compression.

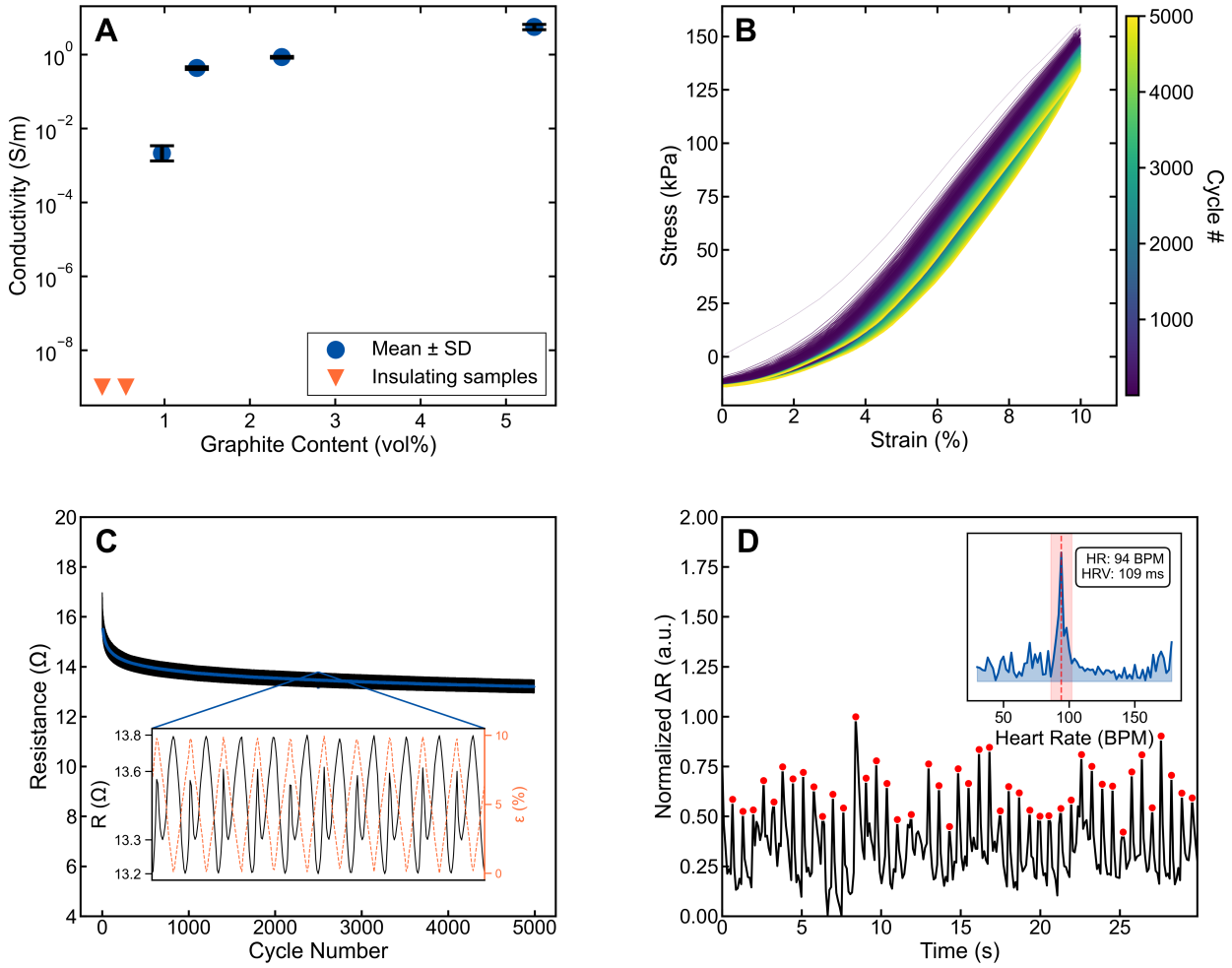


**Figure 2. Electrical and electromechanical characterization of silicone-graphene composite foam.** (A) Through-thickness conductivity versus graphite content showing percolation transition from insulating (<0.6 vol%, orange triangles below detection limit) to conductive regime (≥1.04 vol%, blue circles). (B) Stress-strain hysteresis loops for all 5000 compression cycles (0–10% strain). Color gradient from purple (early cycles) to yellow (late cycles) reveals progressive mechanical conditioning and stiffening. (C) Electrical resistance during 5000 compression cycles showing rapid break-in followed by a stable piezoresistive response. Inset: magnified view of mid-test cycles. (D) Piezoresistive radial pulse sensing. Inset: FFT analysis identifies heart rate at 94 BPM.

Occam's razor dictates that this is a contact resistance issue. However, given the use of silver epoxy as a contact agent, this is unlikely as it is spread as a paste, filling all exposed pores. We propose that when the foam is at rest, graphene sheets coat the cell walls. As we compressed, the pores closed and graphene-rich cell walls came into closer contact, lowering the path length and thus decreasing resistance.[42, 43] When the pores fully closed, we reach a sharp inflection point and transition to a Poisson-type regime where lateral deformation causes junctions between graphene sheets to slip past each other, resulting in an increase in resistance.[44] Beyond this point, further compression caused resistance to increase due to elastic deformations within the foam structure, including cell wall buckling, shearing, and localized folding that

disrupted established conductive pathways.[45] This inflection point suggests a rapid transition where resistance decrease from pore-closing is outcompeted by resistance increase from Poisson-type deformation. When the force is removed, the resistance quickly rebounds to the baseline. Based on our testing, this appears to be independent of deformation with the effect appearing at both 10% and 20% cyclic strains (Figure 2C & S6). This is not unexpected, as the non-monotonic response is a signature of the underlying segregated network, we would expect a unified, monotonic response if the graphene was isotropically dispersed in the underlying matrix. This type of U-shaped response was observed in similar work by Sengupta, Pei, and Kottapalli [44].

For the 10% strain experiment (Figure 2C) the gauge factor was evaluated at 6.68% strain which corresponded to the average inflection point where the piezoresistive response of the foam transitioned from monotonic to U-shaped. In this regime, the material exhibited negative piezoresistive response. The gauge factor was determined to be $-0.61 \pm 0.04$. Long-term cycling revealed an initial break-in period followed by a steady-state regime. During the first 1000 cycles, baseline resistance decreased from 15.5 Ω to 13.0 Ω as mobile graphene sheets formed optimal conductive pathways. Following the initial break-in period the resistance baseline stabilized. The Figure 2C inset provides a magnified view of the resistance change in mid-test cycles. This demonstrates the uniformity of the piezoresistive response.

We performed a similar cyclical compression study using a sample with added chain extender (0.311 mmol vinyl/g from Table S1C) at 20% cyclic compression (up from 10%). In the 20% strain experiment (Figure S6A), we observe the same non-monotonic response. However, our gauge factor was found to be significantly higher, $-4.6 \pm 0.50$ at the inflection point, $n = 9$. The local gauge factor was also studied (Figure S6B&C) which ranged from $-7.6 \pm 1.8$ at 2% strain to $+5.2 \pm 0.5$ at 18% strain. The enhanced sensing ability of this sample was likely derived from addition of a small amount of chain extender resulting in a softer, more readily deformable network.

The responsiveness of the material was also found to be heavily geometry-dependent. When the material was configured as a small strip for surface sensing, sensitivity was amplified. This was demonstrated by monitoring radial pulse (Figure 2D). A thin foam strip was placed on the wrist and resistance was monitored. A distinct peak for each heartbeat was conserved with a 12% change in relative resistance. Fast Fourier Transform (FFT) identified a heart rate of 94 beats per minute. This was validated against an Apple Watch Ultra as well as palpation-based heart rate determination.

## Electrothermal Characterization

The silicone-graphene foam was evaluated for its potential for heating and de-icing applications (Figure 3). Steady state measurements were performed on a planar sample at 1.43% graphene loading at voltages from 0 to 125 V. Figure 3A presents current density vs. temperature data for this voltage series. Current densities of 0–11.9 $mA/cm^3$ resulted in surface temperatures of up to 143 °C. Infrared thermal imaging (Figure S7) confirmed a uniform temperature distribution across the sample surface during Joule heating.

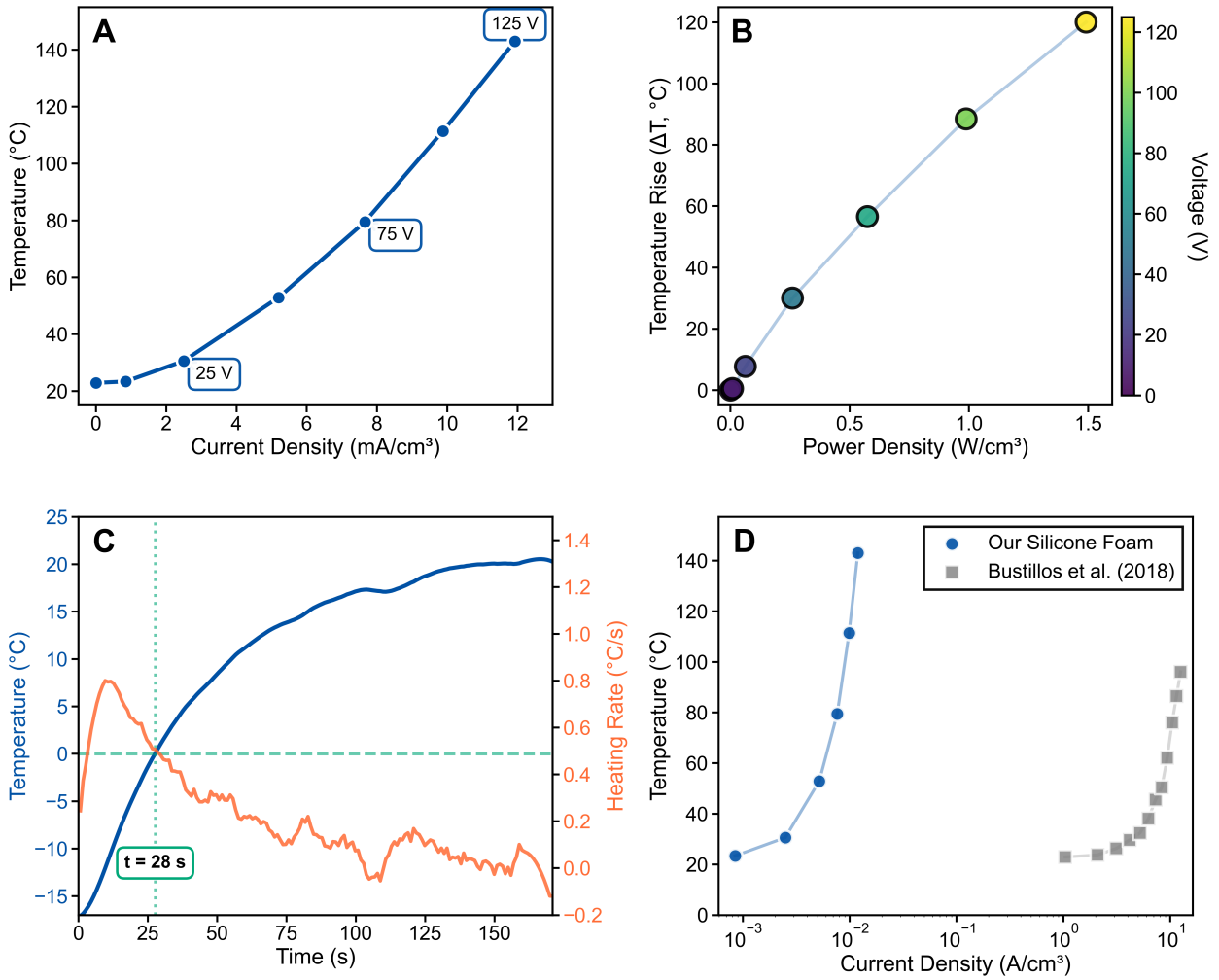


**Figure 3. Electrothermal performance and de-icing characteristics of silicone-graphene foam composite.** (A) Current density versus equilibrium temperature showing the relationship across applied voltages from 0 to 125 V. The current density ranges from 0 to 11.9 mA/cm$^3$, and the equilibrium temperatures range from 22.9°C to 143°C. (B) Power density versus temperature rise (ΔT) relative to the ambient baseline. Marker colors correspond to applied voltage values according to the viridis colorbar (0–125 V), showing power densities from 0 to 1.49 W/cm$^3$ and a temperature rise of up to 120°C. (C) Time-resolved temperature profile (blue line, left y-axis) and instantaneous heating rate (orange line, right y-axis) during heating from an initial temperature of −17°C. The horizontal dashed line marks the freezing point (0°C), and the vertical dotted line indicates the time required to reach 0°C (28 s). (D) Comparison of current density versus temperature for the silicone-graphene foam composite (blue circles) and the graphene foam-epoxy composite from Bustillos et al. [23] (gray squares). Bustillos' data was digitized from the original publication using Plot Digitizer.

The voltage-temperature relationship was near-linear, indicating ohmic conduction through the segregated network, where sheet-to-sheet and pore-to-pore junction resistances dominate electrical transport. The foam exhibits a negative temperature coefficient of resistance (−2122 ppm/°C, Figure S8), consistent with tunneling-dominated conduction through graphene-graphene junctions rather than metallic transport. This temperature dependence must be considered when designing closed-loop heating systems. Figure 3B shows the same underlying data as Figure 3A, but with temperature rising with power density. Data points are colored according to applied voltage (0–125 V, viridis scale). At steady state, the foam required approximately 0.008 W/cm$^3$ per degree at 30 °C, becoming less efficient at 120 °C (0.012 W/cm$^3$ per degree). This efficiency at modest $\Delta T$ suits de-icing, where only the ice-surface interface must melt before bulk ice sheds from the hydrophobic silicone rather than requiring complete melt-through. The transient de-icing behavior of the foam was evaluated in Figure 3C. The composite began at −17 °C and, with 15 W applied, reached 0 °C in 28 seconds. The peak heating rate was 0.80 °C/s, with an average rate of 0.60 °C/s over the first 30 seconds. This reflects the foam

structure: heat generates at graphene-graphene junctions and conducts through air-filled pores and silicone, both poor thermal conductors.

Figure 3D illustrates the difference in operational regime between our composite foam (1.43 vol%) and Bustillos et al. [23] (0.1 vol% loading). Unfortunately, comparison with other silicone-graphene foam systems was not possible due to a lack of publication of electrical data and/or sample dimensions. While we employ a segregated network, Bustillos et al. use a continuous network of graphene foam infiltrated with PDMS. Our silicone-graphene foam operates at current densities of 0.8 to 12 mA/cm$^3$ over temperatures of 25–143 °C. The Bustillos et al. system operates at 1–12.5 A/cm$^3$ across 20–95 °C. The three orders of magnitude disparity is a direct result of the fundamental architectural difference between the segregated network structure (pore wall-confined transport with graphene-PDMS-graphene junction resistance) and the continuous CVD network (uninterrupted transport pathways). The present work achieves a maximum temperature 50 °C higher despite an electrical conductivity approximately 1000 times lower (estimated ~0.4 to ~0.9 S/m versus 400–500 S/m for Bustillos et al.). Because $P = V^2/R$, the foam's high resistance achieves equivalent power dissipation at higher voltage and lower current than continuous graphene networks. At 125 V, the foam draws ~12 mA/cm$^3$; a continuous CVD network achieving the same temperature would require ~10 A/cm$^3$ at much lower voltage. The HIPE-templated segregated network offers a complementary operational regime: low effusivity, high resistivity, low current, and high voltage.

## Conclusions

Thermodynamically driven self-assembly at oil-water interfaces creates segregated graphene networks in minutes using natural flake graphite. This method replaces the 2,500-hour processing required by prior interfacial methods. The foam achieves 0.43 S/m at 1.37 vol% graphene, a 12-fold reduction in filler content compared to previous work, which required 16.5 vol% for comparable conductivity. Emulsion templating confines graphene to cell walls, while the bulk silicone remains largely graphene-free, yielding a porous structure.

This architectural separation enables independent tuning of mechanical and electrical properties, because the conductive network resides at interfaces rather than in the bulk. The same architecture supports both piezoresistive sensing (stable over 5000 cycles) and electrothermal heating to 143 °C at milliamp current densities, three orders of magnitude below those of continuous CVD networks.

## Experimental Section

### Materials

Vinyl-terminated poly(dimethylsiloxane) (DMS-V21), hydride-terminated PDMS chain-extender (DMS-H03), pendant-hydride copolymer cross-linker (HMS-301), and platinum-divinyltetramethyldisiloxane complex (2 wt% Pt in xylene) were purchased from Gelest, Inc. Nano 24 natural flake graphite (median flake size ≈ 1 µm) was acquired from Asbury Carbons. Heptane (lab grade) was acquired from Lab Alley. Deionized water (1 MΩ cm) was used as the internal phase. All reagents were used as received. Dichlorodimethylsilane was acquired from Sigma-Aldrich. MG Chemicals 8331D Silver Conductive Epoxy was acquired from Amazon.

### Silylation of Reaction Vessels

Borosilicate scintillation vials (20 mL) were silanized to minimize foam adhesion. Vials were exposed to a 2% solution of dichlorodimethylsilane for 30 min under ambient laboratory conditions, rinsed with heptane, and dried at 110 °C.

### Preparation of Graphene–Silicone PolyHIPE

A typical recipe for the graphene–silicone polyHIPE foam contains 44.64 g of DMS-V21 (vinyl-terminated silicone macromer), 5.35 g HMS-301 (pendant-hydride cross-linker), 8.08 g of heptane (diluent/exfoliation enhancer), 60.83 g of deionized water (dispersed phase), and 3.25 g of Nano 24 graphite (conductive filler and emulsion stabilizer). Exact formulations for the various experiments are provided in Table S1.

DMS-V21, HMS-301, graphite, deionized water, and heptane were weighed directly into a glass jar. The mixture was hand-shaken vigorously for 1 min to exfoliate graphene and form the emulsion template. Polymerization was initiated by adding 13 drops (~200 ppm relative to the organic phase) of the platinum catalyst solution (SIP6831.2) and shaking for a further 30 s. The solution was then cast into a silylated glass petri dish. Gelation occurred within 2–3 min at ambient

temperature. The sample was demolded with a razor blade, skinned, and dried at 70 °C for approximately 100 hr in a convection oven to remove the dispersed phase.

### SEM Analysis

SEM analysis was performed using a FEI Nova NanoSEM 450 scanning electron microscope. Foam samples were cut using a razor blade. Samples were pinned to SEM stubs (cross-section visible) using copper tape because the samples were non-wettable. Samples were sputter-coated with 5 nm Au/Pd and imaged at 2 kV in Everhart–Thornley detector (ETD) or through-the-lens detector (TLD) mode. Cross sections were imaged.

### Electrical Testing

Foam samples were prepared at varying graphene loading levels (vol% 0.36, 0.66, 1.04, 1.37, 2.22, 4.66; see Table S1A for exact formulation). Foam pieces were sectioned into three rectangular prisms, ~$25 \times 25 \times 10$ mm. Sample densities were determined by measuring the exact sample dimensions with an electronic caliper and the sample mass. Contact resistance was minimized by applying silver epoxy to copper foil sheets approximately $30 \times 30$ mm in size (critically, larger than the sample). Copper wires were placed on the epoxied surface, and the foam sample was placed on top with a 250 g weight to apply pressure during curing, while sandwiching the wires. Alligator clips were used to attach two additional electrodes to the edge of the foil, without contacting the sample. This formed a four-point Kelvin probe setup similar to the technique outlined by Warner and Graf [46]. See Figure S1 for a schematic of this setup.

Conductivity ($\sigma$) was calculated using the equation:

$$\sigma = \frac{L}{R \cdot A} \tag{1}$$

where $L$ is the sample thickness (~10 mm), $R$ is the measured resistance, and $A$ is the cross-sectional area of the specimen (~625 $mm^2$). Volume percentages were calculated using foam densities and a graphite density of 2.26 $g/cm^3$.

### Piezoresistive Characterization

The piezoresistive response of the composite was studied using an Instron 5869 universal testing machine and a Keithley 2400 Source Measure Unit (SMU). The Instron recorded mechanical data. Electrical data was recorded at 10 Hz with a 1 mA test current. Electrical contact was established using the same method detailed in the Electrical Testing section above; however, resistance was measured in a two-wire configuration. The specimen was subjected to 10% compressive strain at a strain rate of 3.33%/s for a total cycle time of 6 seconds over 5,000 cycles. Separately, a different sample was subjected to 20% compressive strain over 10 cycles at 0.63%/s.

For pulse sensing, a thin strip (approximately $25 \times 5 \times 1$ mm) was cut from the material (one side was insulating). Copper tape was used as the electrodes at each end of the strip, with silver epoxy as the contact agent. The strip was lightly placed against the radial artery, insulating side down for measurements, and resistance was measured simultaneously. Resistance data was detrended and normalized. Heart rate was measured on an Apple Watch Ultra as a reference value. Heart rate and heart rate variability (HRV) were calculated using the fast Fourier transform, heart rate corresponding to the dominant peak, and HRV corresponding to peak width.

### Electrothermal Characterization

Room-temperature electrothermal measurements were performed on a silicone–graphene foam specimen synthesized in a planar form in a silylated glass petri dish. Copper wires were embedded in the sample during polymerization, with one at each end, ~70 mm apart. The sample was cut into a rectangular shape measuring approximately $70 \times 58 \times 2$ mm. A Keithley 2400 SMU was used to apply and measure voltages ranging from 0 to 125 V through the copper wires. Surface temperatures were measured using an infrared thermometer (Traceable, Fisher Scientific) after a 20-minute equilibration period at each voltage step.

### De-icing Experiments

De-icing performance was evaluated using a separate specimen (approximately $25 \times 25 \times 10$ mm, 2.17 vol% graphene loading) precooled in a Tenney Junior environmental chamber (TJR) set to −20 °C. Temperature was monitored using a K-type thermocouple that penetrated the specimen surface, with data acquisition at 1 Hz. After equilibration to −17 °C,

a constant power of approximately 15 W (17.7 V, 0.85 A) was applied using the Keithley 2400 SMU. Time-resolved temperature profiles were recorded to characterize both the de-icing transient and the approach to steady-state.

### Temperature Coefficient of Resistance

Temperature-dependent resistance was measured using a Tenney Junior environmental chamber (TJR). Specimen temperature was monitored with a K-type thermocouple in direct contact with the foam surface, while resistance was recorded simultaneously using a Keithley 2400 SMU. Measurements were taken at 1-second intervals across a temperature range of −67 °C to 180 °C.

**Supporting Information**

Formulation compositions for all sample series (Table S1); four-point probe measurement configuration (Figure S1); sphere size distribution analysis including cumulative, volume fraction, and number fraction distributions (Figure S2); additional SEM micrographs of foam morphology (Figure S3); photograph of competitive silica adsorption at the oil-water interface (Figure S4); crosslink density effects on mechanical properties (Figure S5); piezoresistive response under cyclic compression (Figure S6); infrared thermal imaging of electrothermal heating at multiple voltages (Figure S7); temperature-dependent resistance from −67 °C to 180 °C (Figure S8).

**Author Contributions**

B.F. designed and performed experiments, analyzed data, and wrote the manuscript. D.H.A. conceived the project, supervised the research, and edited the manuscript.

**Acknowledgements**

The authors thank Dr. Xuanhao Sun for assistance with scanning electron microscopy. The authors thank the USDA for their support through grant #221470. The authors thank Asbury Carbons for providing the natural flake graphite used in this study.

**Conflict of Interest**

The authors declare no competing financial interests.

**Data Availability**

The data that support the findings of this study are available from the corresponding author upon reasonable request.

## References

[1] John A. Rogers, Takao Someya, and Yonggang Huang. “Materials and Mechanics for Stretchable Electronics”. In: *Science* 327.5973 (2010), pp. 1603–1607. DOI: 10.1126/science.1182383.

[2] Naoji Matsuhisa et al. “Materials and structural designs of stretchable conductors”. In: *Chemical Society Reviews* 48.11 (2019), pp. 2946–2966. DOI: 10.1039/C8CS00814K.

[3] Samuel E. Root et al. “Mechanical Properties of Organic Semiconductors for Stretchable, Highly Flexible, and Mechanically Robust Electronics”. In: *Chemical Reviews* 117.9 (2017), pp. 6467–6499. DOI: 10.1021/acs.chemrev.7b00003.

[4] Soonjae Pyo et al. “Recent Progress in Flexible Tactile Sensors for Human-Interactive Systems: From Sensors to Advanced Applications”. In: *Advanced Materials* 33.47 (2021), p. 2005902. DOI: 10.1002/adma.202005902.

[5] Kaichen Xu, Yuyao Lu, and Kuniharu Takei. “Flexible Hybrid Sensor Systems with Feedback Functions”. In: *Advanced Functional Materials* 31.39 (2021), p. 2007436. DOI: 10.1002/adfm.202007436.

[6] Jiangxin Wang et al. “Deformable conductors for human–machine interface”. In: *Materials Today* 21.5 (2018), pp. 508–526. DOI: 10.1016/j.mattod.2017.12.006.

[7] G. Deshpande and M. E. Rezac. “Kinetic Aspects of the Thermal Degradation of Poly(Dimethyl Siloxane) and Poly(Dimethyl Diphenyl Siloxane)”. In: *Polymer Degradation and Stability* 76.1 (2002), pp. 17–24. DOI: 10.1016/S0141-3910(01)00261-0.

[8] Shaopeng Li et al. “Functional PDMS Elastomers: Bulk Composites, Surface Engineering, and Precision Fabrication”. In: *Advanced Science* 10.34 (2023), p. 2304506. DOI: 10.1002/advs.202304506.

[9] Mert Vural et al. “Spray-Processed Composites with High Conductivity and Elasticity”. In: *ACS Applied Materials & Interfaces* 10.16 (2018), pp. 13953–13962. DOI: 10.1021/acsami.8b00068.

[10] A J Marsden et al. “Electrical percolation in graphene–polymer composites”. In: *2D Materials* 5.3 (2018), p. 032003. DOI: 10.1088/2053-1583/aac055.

[11] Wolfgang Bauhofer and Josef Z. Kovacs. “A review and analysis of electrical percolation in carbon nanotube polymer composites”. In: *Composites Science and Technology* 69.10 (2009), pp. 1486–1498. DOI: 10.1016/j.compscitech.2008.06.018.

[12] Ermias Wubete Fenta and Berihun Abebaw Mebratie. “Advancements in carbon nanotube-polymer composites: Enhancing properties and applications through advanced manufacturing techniques”. In: *Heliyon* 10.16 (2024). DOI: 10.1016/j.heliyon.2024.e36490.

[13] Rahul Rao et al. “Carbon Nanotubes and Related Nanomaterials: Critical Advances and Challenges for Synthesis toward Mainstream Commercial Applications”. In: *ACS Nano* 12.12 (2018), pp. 11756–11784. DOI: 10.1021/acsnano.8b06511.

[14] Jose Enrico Q. Quinsaat et al. “Conductive silicone elastomers electrodes processable by screen printing”. In: *Scientific Reports* 9.1 (2019), p. 13331. DOI: 10.1038/s41598-019-49939-8.

[15] Yenny Hernandez et al. “High-yield production of graphene by liquid-phase exfoliation of graphite”. In: *Nature Nanotechnology* 3.9 (2008), pp. 563–568. DOI: 10.1038/nnano.2008.215.

[16] Sung-Hoon Park et al. “Modeling the electrical resistivity of polymer composites with segregated structures”. In: *Nature Communications* 10.1 (2019), p. 2537. DOI: 10.1038/s41467-019-10514-4.

[17] Lekshmi A. Kurup et al. “Graphene Porous Foams for Capacitive Pressure Sensing”. In: *ACS Applied Nano Materials* 5.2 (2022), pp. 2973–2983. DOI: 10.1021/acsanm.2c00247.

[18] Yu Long et al. “A porous graphene/polydimethylsiloxane composite by chemical foaming for simultaneous tensile and compressive strain sensing”. In: *FlatChem* 10 (2018), pp. 1–7. DOI: 10.1016/j.flatc.2018.07.001.

[19] Ying Wu et al. “Highly Aligned Graphene Aerogels for Multifunctional Composites”. In: *Nano-Micro Letters* 16.1 (2024), p. 118. DOI: 10.1007/s40820-024-01357-w.

[20] Zhenyu Wang et al. “Highly stretchable graphene/polydimethylsiloxane composite lattices with tailored structure for strain-tolerant EMI shielding performance”. In: *Composites Science and Technology* 206 (2021), p. 108652. DOI: 10.1016/j.compscitech.2021.108652.

[21] Marcus A. O’Mara et al. “Ultrasensitive Strain Gauges Enabled by Graphene-Stabilized Silicone Emulsions”. In: *Advanced Functional Materials* 30.32 (2020), p. 2002433. DOI: 10.1002/adfm.202002433.

[22] Sean P. Ogilvie et al. “Nanosheet-Stabilized Emulsions: Near-Minimum Loading and Surface Energy Design of Conductive Networks”. In: *ACS Nano* 16.2 (2022), pp. 1963–1973. DOI: 10.1021/acsnano.1c06519.

[23] Jenniffer Bustillos et al. “Three-Dimensional Graphene Foam–Polymer Composite with Superior Deicing Efficiency and Strength”. In: *ACS Applied Materials & Interfaces* 10.5 (2018), pp. 5022–5029. DOI: 10.1021/acsami.7b18346.

[24] Ji-Hwan Ha et al. “Development of Multi-Functional Graphene Polymer Composites Having Electromagnetic Interference Shielding and De-Icing Properties”. In: *Polymers* 11.12 (2019), p. 2101. DOI: 10.3390/polym11122101.

[25] Steven J. Woltornist et al. “Conductive Thin Films of Pristine Graphene by Solvent Interface Trapping”. In: *ACS Nano* 7.8 (2013), pp. 7062–7066. DOI: 10.1021/nn402371c.

[26] Elizabeth E.B. Brown, Steven J. Woltornist, and Douglas H. Adamson. “PolyHIPE foams from pristine graphene: Strong, porous, and electrically conductive materials templated by a 2D surfactant”. In: *Journal of Colloid and Interface Science* 580 (2020), pp. 700–708. DOI: 10.1016/j.jcis.2020.07.026.

[27] Steven J. Woltornist et al. “Polymer/Pristine Graphene Based Composites: From Emulsions to Strong, Electrically Conducting Foams”. In: *Macromolecules* 48.3 (2015), pp. 687–693. DOI: 10.1021/ma5024236.

[28] Steven J. Woltornist et al. “Controlled 3D Assembly of Graphene Sheets to Build Conductive, Chemically Selective and Shape-Responsive Materials”. In: *Advanced Materials* 29.18 (2017), p. 1604947. DOI: 10.1002/adma.201604947.

[29] Kirill Efimenko, William E. Wallace, and Jan Genzer. “Surface Modification of Sylgard-184 Poly(dimethyl siloxane) Networks by Ultraviolet and Ultraviolet/Ozone Treatment”. In: *Journal of Colloid and Interface Science* 254.2 (2002), pp. 306–315. DOI: 10.1006/jcis.2002.8594.

[30] R. Pichot, F. Spyropoulos, and I. T. Norton. “Competitive adsorption of surfactants and hydrophilic silica particles at the oil–water interface: Interfacial tension and contact angle studies”. In: *Journal of Colloid and Interface Science* 377.1 (2012), pp. 396–405. DOI: 10.1016/j.jcis.2012.01.065.

[31] Jennifer Kane, Jason Ong, and Ravi F. Saraf. “Chemistry, physics, and engineering of electrically percolating arrays of nanoparticles : a mini review”. In: *Journal of Materials Chemistry* 21.42 (2011), pp. 16846–16858. DOI: 10.1039/C1JM12005K.

[32] Konrad Schwenke, Lucio Isa, and Emanuela Del Gado. “Assembly of Nanoparticles at Liquid Interfaces: Crowding and Ordering”. In: *Langmuir* 30.11 (2014), pp. 3069–3074. DOI: 10.1021/la404254n.

[33] Sohaib Mohammed et al. “Self-Assembly of Silica Nanoparticles at Water–Hydrocarbon Interfaces: Insights from In Operando Small-Angle X-ray Scattering Measurements and Molecular Dynamics Simulations”. In: *Energy & Fuels* 34.10 (2020), pp. 12545–12555. DOI: 10.1021/acs.energyfuels.0c02759.

[34] V. M. Gun’ko et al. “Influence of the Partial Hydrophobization of Fumed Silica by Hexamethyldisilazane on Interactions with Water”. In: *Langmuir* 19.26 (2003), pp. 10816–10828. DOI: 10.1021/la0301238.

[35] D. B. Mahadik et al. “Effect of concentration of trimethylchlorosilane (TMCS) and hexamethyldisilazane (HMDZ) silylating agents on surface free energy of silica aerogels”. In: *Journal of Colloid and Interface Science* 356.1 (2011), pp. 298–302. DOI: 10.1016/j.jcis.2010.12.088.

[36] Joeri Smits et al. “Synergistic and Competitive Adsorption of Hydrophilic Nanoparticles and Oil-Soluble Surfactants at the Oil–Water Interface”. In: *Langmuir* 37.18 (2021), pp. 5659–5672. DOI: 10.1021/acs.langmuir.1c00559.

[37] Tommy S. Horozov, Bernard P. Binks, and Torsten Gottschalk-Gaudig. “Effect of electrolyte in silicone oil-in-water emulsions stabilised by fumed silica particles”. In: *Physical Chemistry Chemical Physics* 9.48 (2007), pp. 6398–6404. DOI: 10.1039/B709807N.

[38] Chaoxuan Shen et al. “Silica coating onto graphene for improving thermal conductivity and electrical insulation of graphene/polydimethylsiloxane nanocomposites”. In: *Journal of Materials Science & Technology* 35.1 (2019), pp. 36–43. DOI: 10.1016/j.jmst.2018.09.016.

[39] Lance Kersey et al. “The effect of adhesion promoter on the adhesion of PDMS to different substrate materials”. In: *Lab on a Chip* 9.7 (2009), pp. 1002–1004. DOI: 10.1039/B813757A.

[40] Steven P. Koenig et al. “Ultrastrong adhesion of graphene membranes”. In: *Nature Nanotechnology* 6.9 (2011), pp. 543–546. DOI: 10.1038/nnano.2011.123.

[41] Yasser Zare, Nima Gharib, and Kyong Yop Rhee. “Influences of Tunneling Distance and Interphase Size on the Conductivity of Graphene-Filled Nanomaterials”. In: *JOM* (2023). DOI: 10.1007/s11837-023-05932-1.

[42] Yuyang Qin et al. “Lightweight, Superelastic, and Mechanically Flexible Graphene/Polyimide Nanocomposite Foam for Strain Sensor Application”. In: *ACS Nano* 9.9 (2015), pp. 8933–8941. DOI: 10.1021/acsnano.5b02781.

[43] Hong-Bin Yao et al. “A Flexible and Highly Pressure-Sensitive Graphene–Polyurethane Sponge Based on Fractured Microstructure Design”. In: *Advanced Materials* 25.46 (2013), pp. 6692–6698. DOI: 10.1002/adma.201303041.

[44] Debarun Sengupta, Yutao Pei, and Ajay Giri Prakash Kottapalli. “Ultralightweight and 3D Squeezable Graphene-Polydimethylsiloxane Composite Foams as Piezoresistive Sensors”. In: *ACS Applied Materials & Interfaces* 11.38 (2019), pp. 35201–35211. DOI: 10.1021/acsami.9b11776.

[45] Zilu Wang et al. “Electrical Conductivity of Graphene–Polymer Composite Foams: A Computational Study”. In: *Macromolecules* 52.19 (2019), pp. 7379–7385. DOI: 10.1021/acs.macromol.9b01669.

[46] Terence E. Warner and Thomas Graf. “On the measurement of the electrical conductivity of graphite-polymer composite bipolar plates”. In: *Journal of Power Sources* 594 (2024), p. 233871. DOI: 10.1016/j.jpowsour.2023.233871.

**Table of Contents**

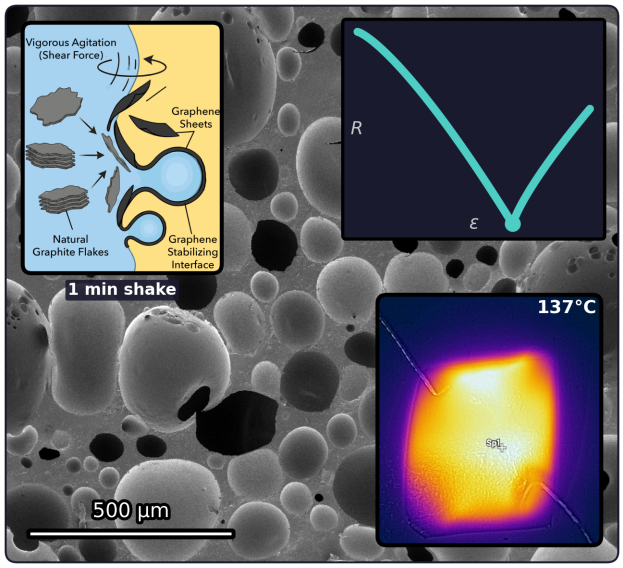


Graphene-silicone composite foams are synthesized in minutes through thermodynamically driven self-assembly at oil-water interfaces. Natural graphite exfoliates and localizes at emulsion boundaries, creating segregated conductive networks achieving 0.43 S/m at just 1.37 vol% loading, a 12-fold reduction versus prior methods. The foams exhibit dual functionality: piezoresistive strain sensing stable over 5000 cycles and electrothermal heating to 143 °C.